Biophysical Journal, Volume 98

Supporting Material

Structural hierarchy governs fibrin gel mechanics

Izabela K. Piechocka, Rommel G. Bacabac, Max Potters, Fred C. MacKintosh, and Gijsje H. Koenderink

SUPPORTING MATERIALS

Note S1. Calculations of fiber persistence length based on a bundle model

The persistence length of a fibrin fiber can be estimated in a number of different ways. A coarse-grained approach is to model the fiber as a homogeneous, isotropic cylinder with radius r and Young's modulus E. The persistence length is then given as:

$$L_p = \frac{EI}{k_B T}, \tag{S1}$$

where $I = \pi r^4/4$ is the moment of inertia and $k_B T$ denotes thermal energy, where k_B is the Boltzmann constant and T is absolute temperature. The Young's modulus of fibrin has been measured by bending and stretching of individual fibers within fibrin clots using optical tweezers (1). Using values of E between 2 MPa (unligated fibers) and 15 MPa (ligated fibers), l_p of a fiber with a diameter of 100 nm would be 2-17 mm.

An alternative estimate of l_p can be obtained by taking into account that the fiber is a bundle of N wormlike protofibrils, each having a persistence length l_p^{pf} of 0.5 μm (2, 3). The effective persistence length of such a bundle depends on the resistance of the crosslinks between the protofibrils to shearing (4, 5). When the crosslinks strongly resist shear and rigidly glue the protofibrils together (fully coupled regime), the bundle behaves as a homogeneous beam and $l_p = N^2 l_p^{pf}$. On the other hand, when the crosslinks do not resist shear and 'tilt' freely during bundle bending (decoupled bending), the protofibrils bend independently and $l_p = N l_p^{pf}$. Since crosslinks in general have a finite shear stiffness, l_p is expected to eventually crossover from N^2 scaling to N scaling with increasing N. The importance of crosslink shearing depends on several molecular parameters, including the axial spacing between crosslinks, the shear stiffness of the crosslinks, and the extensional stiffness of the protofibrils. For a bundle of $N = 65$ protofibrils (as in our experiments), l_p is 33 μm in the decoupled limit and 1.5 mm in the fully coupled limit.

Note S2. Determination of fiber size by turbidimetry

Fiber diameters, d, and mass-length ratios, μ, were measured by turbidimetry, using a UV1 Spectrophotometer (Thermo Optek). The turbidity,

$\tau = (1/l)\ln(1/T)$, where l is the path length in cm (here 1 cm) and T is the measured transmission. The diameter was extracted from the dependence of τ on wavelength, λ, between 350-650 nm, following the method of Carr and Hermans (10). When the fiber radius is much smaller than λ, τ scales as λ^{-3}, and the slope is proportional to the mass-length ratio, μ. This proportionality is not observed for our clots, indicating that the fiber diameter is not negligible compared to λ. This is consistent with the observation with AFM that the fiber diameter is on the order of 100 nm. When the fiber radius is similar to λ, μ and d are obtained instead by plotting $c/\tau\lambda^3$ versus λ^{-2}. The intercept of this plot is equal to A/μ, where $A = 0.68{\cdot}10^{23}$ is a material constant (expressing λ in cm and c_p in g/cm^3). The ratio of slope and intercept is proportional to the square of the fiber radius, Br^2, with $B/A = 20.9$ a material constant. Our networks fall into the second category, with $c/\tau\lambda^3$ scaling as λ^{-2} (Fig. S1 A).

Note S3. Calculation of persistence length of fibers from single filament fluctuations at high frequencies

The viscoelastic response of semiflexible polymer networks at high frequencies can be used to measure the polymer persistence length. At high frequencies the shear modulus is controlled by the relaxation of individual polymer chains, leading to the characteristic response (6, 7):

$$G^*(\omega) = \frac{1}{15}\rho\kappa l_p(-2i\zeta/\kappa)^{3/4}\omega^{3/4} - i\omega\eta, \tag{S2}$$

where ρ is the filament length per volume, $\kappa = l_p k_B T$ is the bending stiffness, $\zeta = 4\pi\eta/ln(0.6\lambda/d)$ is the lateral drag coefficient and η is the solvent viscosity at 37 °C. Using for λ the characteristic mesh size, we find $l_p = 60$ μm for our fibers.

It is possible that our microrheology experiments measure direct fiber motion, since the bead sizes used are comparable to the mesh size of the network, and since our beads bind to the fibers. Such motion is expected to be dominated by the transverse motion of fibers, which is also predicted to exhibit the same qualitative dynamics that we observe: the transverse motion is also characterized by the same 3/4 exponent in either time or frequency dependence (8, 9):

$$\langle(\triangle h(t))^2\rangle \simeq 0.082\ \{ln\ [\frac{\kappa ln(\frac{L}{\pi a})t}{4\pi\eta a^4}]\ (\frac{k_BT}{\kappa})^{1/3}\ \frac{k_BT}{\eta}t\}^{4/3} \tag{S3}$$

If this were the origin of our observations, the corresponding persistence length would be 20 μm. However, if the bead measures fiber fluctuations, the bead fluctuations are expected to be anisotropic, contrary to our observations. Furthermore, the apparent elastic shear modulus derived from the bead fluctuations is close to the bulk modulus. Thus, we believe that our microrheology results measure network rheology. In either case, our experiments clearly indicate significant thermal fluctuations.

Note S4. Calculations of the protofibril stretch modulus

For an isotropic network of fibers with stretch modulus κ_s, $K_s = 1/15\rho\kappa_s$ (6, 7). Using κ_s as an adjustable parameter, we find good agreement with our data for $\kappa_s = 21$ nN. This corresponds to a stretch modulus of 320 pN per protofibril, which is higher than values of 50-100 pN that were found for protofibril gels polymerized from fish fibrinogen (2). However, we expect significant filament alignment in the stretch regime, which is not captured by the isotropic approximation. This alignment means that a larger fraction of filaments bears the load imposed by the applied stress. Thus, the actual force per fiber will be lower than the above. For comparison, for a highly aligned network, we can estimate the macroscopic modulus as $1/8\rho\kappa_s$, based on the following. For a small strain increment $\delta\gamma$, the stress contribution due to a filament oriented with polar angle θ relative to the vertical axis and azimuthal angle ϕ is given by $\delta\sigma = \rho \sin\theta \cos\theta \cos\phi\kappa_s\delta\epsilon$, where the extensional strain of the filament is $\delta\epsilon = \sin\theta\cos\theta\cos\phi\delta\gamma$. Under shear, approximately half of the filaments will experience stretching, while the other half experiences compression. The latter will tend to buckle under shear and will not contribute to the macroscopic stress (11–13), while diagonal filaments, such as the one indicated in the inset to Fig. 2A, will bear most of the load. Thus, assuming half of the filaments is oriented so as to stretch and bear the load, we obtain $\delta\sigma \simeq 1/4\rho\kappa_s\delta\epsilon = 1/8\rho\kappa_s\delta\gamma$. This results in $K_s = 1/8\rho\kappa_s$ and a somewhat smaller value for κ_s of about 170 pN, in better agreement with ref. (2).

References

[1] Collet, J., H. Shuman, R. Ledger, S. Lee, and J. Weisel. 2005. The elasticity of an individual fibrin fiber in a clot. *PNAS*. 102:9133–9137.

[2] Storm, C., J. Pastore, F. MacKintosh, T. Lubensky, and P. Janmey. 2005. Nonlinear elasticity in biological gels. *Nature*. 435:191–194.

[3] Wen, Q., A. Basu, J. Winer, A. Yodh, and P. Janmey. 2007. Local and global deformations in a strain-stiffening fibrin gel. *New J Phys*. 9:428.

[4] Claessens, M., M. Bathe, E. Frey, and A. Bausch. 2006. Actin-binding proteins sensitivelymediate F-actin bundle stiffness. *Nat Mater*. 5:748–753.

[5] Bathe, M., C. Heussinger, M. Claessens, A. Bausch, and E. Frey. 2008. Cytoskeletal bundle mechanics. *Biophys J*. 94:2955–2964.

[6] Gittes, F., and F. MacKintosh. 1998. Dynamic shear modulus of a semiflexible polymer network. *Phys Rev E*. 58:R1241–R1244.

[7] Morse, D. 1998. Viscoelasticity of tightly entangled solutions of semiflexible polymers. *Phys Rev E*. 58:R1237–R1240.

[8] Farge, E., and A. Maggs. (1993) Dynamic scattering from semiflexible polymers. *Macromolecules*. 26:5041–5044.

[9] Granek, R. 1997. From semi-flexible polymers to membranes: Anomalous diffusion and reptation. *J Phys II*. 7:1761–1788.

[10] Carr, M., and J. Hermans. 1978. Size and density of fibrin fibers from turbidity. *Macromolecules*. 11:46–50.

[11] Onck, P., T. Koeman, T. van Dillen, and E. van der Giessen. 2005. Alternative explanation of stiffening in cross-linked semiflexible networks. *Phys Rev Lett*. 95:178102.

[12] Heussinger, C., M. Bathe, and E. Frey. 2007. Statistical mechanics of semiflexible bundles of wormlike polymer chains. *Phys Rev Lett*. 99:048101.

[13] Conti, E., and F. MacKintosh. 2009. Cross-linked networks of stiff filaments exhibit negative normal stress. *Phys Rev Lett*. 102:088102.

[14] Yao, N., R. J. Larsen, and D. Weitz. 2008. Probing nonlinear rheology with inertio-elastic oscillations. *J Rheol.* 52:1013–1025.

[15] Baravian, C., and D. Quemada. 1998. Using instrumental inertia in controlled stress rheometry. *Rheol Acta.* 37:223–233.

[16] Ewoldt, R., and G. McKinley. 2007. Creep ringing in rheometry or how to deal with oft-discarded data in step stress tests. *Rheology Bulletin.* 76:4–24.

[17] Liu, J., K. E. Kasza, G. H. Koenderink, D. Vader, C. P. Broedersz, et al. (preprint, www.seas.harvard.edu/projects/weitzlab/publications.html). Microscopic origins of nonlinear elasticity of biopolymer networks.

Supporting Figures

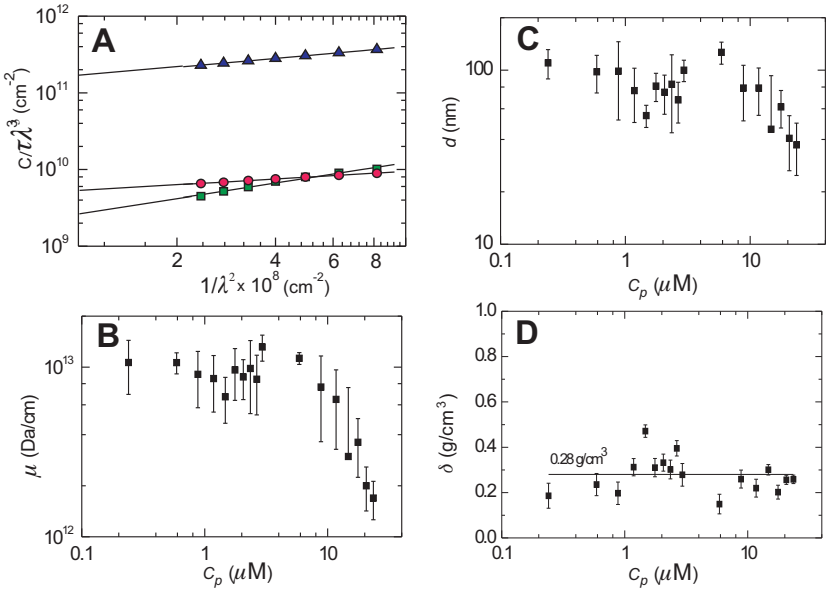

Figure S 1: Turbidity measurements on fibrin gels. (A) Wavelength dependence of the turbidity of 1.5 μM (squares), 3 μM (circles), and 15 μM (triangles) fibrin networks. Straight lines were fitted to the data to allow calculation of mass-length ratio that is proportional to the intercept of these lines and fiber diameter obtained from the ratio of slope and intercept. (B) Mass-length ratio is independent of fibrinogen concentration up to 10 μM and after decreases. (C) Corresponding concentration dependence of fiber diameter. (D) The protein mass density within the fibers remains constant and low (symbols), at about 0.28 g/cm^3 (line), similar to previous observations (10).

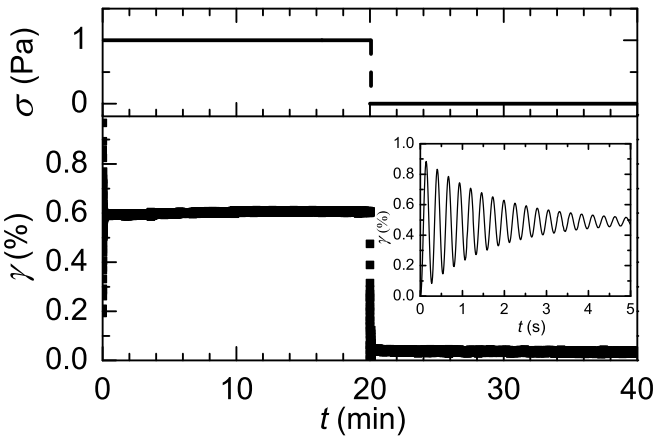

Figure S 2: Time dependence of shear strain (*Bottom*) after imposition and subsequent removal of a steady shear stress (*Top*) for a network of 6 μM fibrin. After imposition of a constant stress, the fibrin network shows a very fast strain response with no subsequent creep. This characteristic solid-like behavior was observed for all fibrin networks. When the stress is released, an immediate and nearly complete recovery of the strain takes place. This suggests that the sample is predominantly elastic. At the beginning of a creep test, the strain response has a superposed damped oscillation (*Inset*). This inertio-elastic oscillation is characteristic for highly elastic materials (14–16).

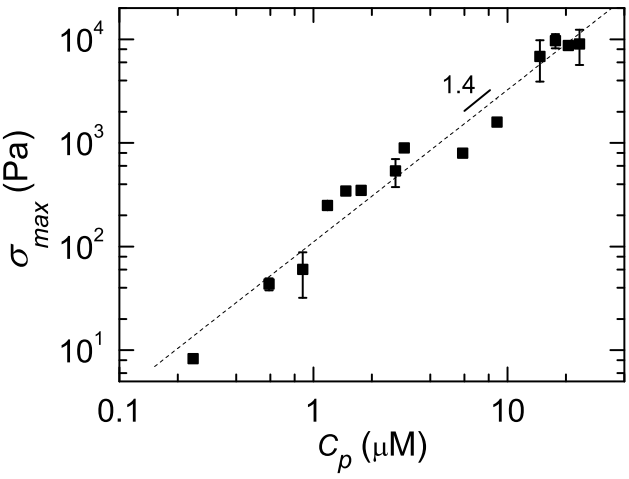

Figure S 3: Concentration dependence of rupture stress. Dashed line indicates power-law fit.

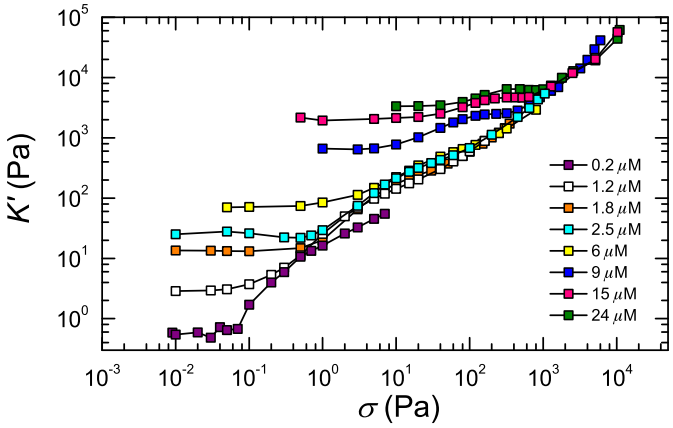

Figure S 4: Stress-stiffening curves for fibrin networks with concentrations as indicated. The stiffening response becomes weaker with increasing fibrinogen concentration.

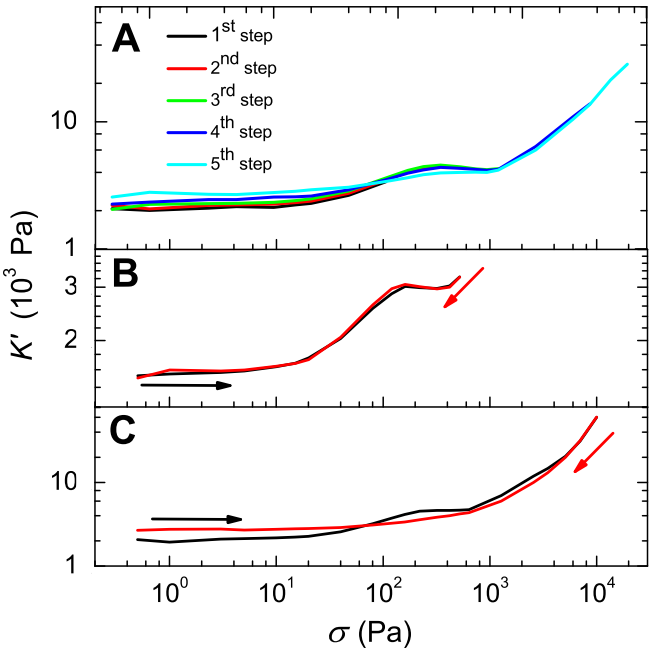

Figure S 5: Repeatability of stress-stiffening curves for 15 μM fibrin network. (A) Stress-stiffening curves were repeatable during many consecutive stress sweeps in the nonlinear regime, even when the stress was brought up almost to the breakage point. Occasionally the stiffness in the linear regime increased after a previous stress sweep. This work-hardening phenomenon is reminiscent of the behavior of actin networks crosslinked by filamin, where it was explained by alignment and bundling of filaments at large strain (17). (B) The stiffening curves obtained by gradually increasing the applied stress were indistinguishable from curves obtained by gradually decreasing the applied stress. (C) Only when the samples were subjected to strains close to the rupture strain, some hysteresis was observed.